crystals

MDPI

Article

A New Anti-Alias Model of Ab Initio Calculations of the Generalized Stacking Fault Energy in Face-Centered Cubic Crystals

Dawei Fan [1,2], Qingzhou Zhang [1,2], Touwen Fan [3], Mengdong He [2] and Linghong Liu [1,2,*]

[1] Hunan Province Key Laboratory of Materials Surface and Interface Science and Technology, Central South University of Forestry and Technology, Changsha 410004, China
[2] College of Science, Central South University of Forestry and Technology, Changsha 410004, China
[3] College of Science, Hunan Institute of Technology, Hengyang 421002, China
* Correspondence: t20060971@csuft.edu.cn

Abstract: The anti-alias model is an effective method to calculate the generalized stacking fault energy of the hexagonal close-packed crystals, but it has not been applied to the face-centered cubic crystals due to two different stacking faults occurring in the supercell during the sliding process. Based on the symmetry of these two stacking faults and the existing single analytic formula of the generalized stacking fault energy, we successfully extend the anti-alias model to compute the generalized stacking fault energy of face-centered cubic crystals, and the common fcc metals Al, Ni, Ag and Cu are taken as specific examples to illustrate the computational details. Finally, the validity of the proposed model is verified by data comparison and analysis. It is suggested that the anti-alias model is a good choice for the researchers to obtain more accurate generalized stacking fault energy of face-centered cubic metals.

Keywords: generalized stacking fault energy; anti-alias method; first-principles calculations

check for updates

Citation: Fan, D.; Zhang, Q.; Fan, T.; He, M.; Liu, L. A New Anti-Alias Model of Ab Initio Calculations of the Generalized Stacking Fault Energy in Face-Centered Cubic Crystals. *Crystals* **2023**, *13*, 461. https://doi.org/10.3390/cryst13030461

Academic Editor: Thomas M. Klapötke

Received: 20 January 2023
Revised: 21 February 2023
Accepted: 3 March 2023
Published: 8 March 2023

Copyright: © 2023 by the authors. Licensee MDPI, Basel, Switzerland. This article is an open access article distributed under the terms and conditions of the Creative Commons Attribution (CC BY) license (https://creativecommons.org/licenses/by/4.0/).

1. Introduction

With the increasing requirement for better strength or ductility of materials, the researchers make every effort they can, such as adjusting alloy composition and changing heat treatment and deformation methods, to improve the comprehensive properties of materials [1,2]. Crystal defects such as dislocations and twins play critical roles in plastic deformation and ultimately govern the multifarious mechanical behaviors of many crystalline materials [3]. Face-centered cubic (fcc) metals are polycrystals composed of a large number of grains. The atoms within the grain are arranged in an orderly sequence. When the crystal is subjected to external resistance, the atoms inside the crystal are transported through the dislocation motion, which is easy to slip along the slip plane (close-packed plane), reducing the deformation resistance of the crystal. Multiple slip surfaces are clustered into slip zones, and multiple slip bands are gathered together to form a macroscopic, visible deformation. Dislocation slip and twinning are two important mechanisms in the plastic deformation of face-centered cubic metals [4,5]. Stacking fault (SF) is an important type of planar defect caused by the incorrect stacking sequence of lattice planes in a crystal. The energy difference obtained by shearing two adjacent atomic planes about each other is the stacking fault energy (SFE). It is a critical intrinsic material parameter that significantly affects the plastic deformation behavior and mechanical properties. In general, twinning is often produced in materials with low intrinsic stacking fault energy γ_I (ISFE), such as austenitic steel, Ag and so on. Therefore, γ_I has been traditionally used to describe the difficulty of the deformation twin formed in the materials [6]. However, it was reported that a lot of deformation twins appeared in Ir crystal with a higher ISFE than Al [7]. Therefore, it is not comprehensive enough to estimate the twin deformation ability of materials only with a single physical

quantity of the ISFE. In 1968, Vitek proposed the concept of generalized stacking fault energy (GSFE): a measure of the energy penalty between two adjacent planes during shear deformation in a specific slip direction on a given slip plane, also known as the γ plane [8].

Since the conception of GSFE was proposed, it has been widely used to study the deformation model of crystals. For each lattice type, there exist a number of experimentally observed slip systems characteristic of the crystal symmetry. The fcc crystals have 12 slip systems, and due to the large number of slip systems, the fcc crystals have a large tendency to slip. The plastic deformation is mainly completed by slip, so the fcc crystals have good plasticity. However, twinning is not common for many fcc crystals and alloys. In addition, if the deformation mechanism changes from slip to twin during plastic deformation, their tensile strength and ductility can be increased at the same time.

There are many important characteristic energies on the GSFE curve [9–12], such as intrinsic stacking fault energy (γ_{I}), unstable stacking fault energy (γ_{U}) and unstable twin stacking fault energy (γ_{UT}), which represent the characteristics of plastic deformation. The GSFE curve and the associated characteristic energies can be used to model a vast number of phenomena linked to dislocation slipping, plastic deformation, crystal growth, phase transition and twin-twin interactions, and these phenomena are also present in organic crystals [13–19]. For example, the kinetic process of partial dislocation movements such as cross-slip and climb is controlled by γ_{I}, and $\gamma_{\mathrm{I}} \propto 1/\mathrm{D}$, where D is the width of separation between partial dislocations [20,21]. γ_{U} is the first extremal point along the GSFE curves, represents the barrier that has to be overcome to nucleate a leading partial dislocation and plays a key role in the fracture of the crystal [9,22]. Swygenhoven et al. [23] suggested that the dislocation activity in a simulation is dominated by extended partials or full dislocations traveling through the grains in the simulated time span and must be understood in terms of $\gamma_{\mathrm{I}}/\gamma_{\mathrm{U}}$. Tadmor and Bernstein [24] presented a measure of twinnability as a function of GSFE energies, including the γ_{I}, γ_{U} and γ_{UT} and it was applied to study the twinning tendency of Ag, Al, Au, Cu, Ir, Pb, Pd and Pt metals, which are consistent with the experimental results. Later, the criterion was widely used to study the plastic deformation of materials [25,26]. Then, Asaro and Suresh [27] proposed a twinnability criteria T_{AS} based on the assumption that grain boundaries are the sources for dislocation nucleation. Cai et al. [4] have proposed a twinnability parameter (T_{OR}) involving the energy barriers and assuming homogenous nucleation of dislocations induced by external stress. The high twinnability indicates a greater tendency to twin. Several pure fcc elements and a few binary alloys were ranked using different twinnability criteria (T_{BT}, T_{AS} and T_{OR}) obtained similar results. These criteria only depend on the relative magnitudes of γ_{I}, γ_{U} and γ_{UT}. In addition, the GSFE is the increment of energy due to the misfit interaction, and the atomic interactions in crystals are short ranged. Therefore, the GSFE is highly localized and mainly depends on the atoms near the slip plane. The restoring force can be obtained by taking a derivative of GSFE with respect to displacement, which greatly promotes the Peierls–Nabarro theory.

Among the generalized stacking faults (GSF) of fcc crystals, people are more concerned with the <11$\bar{2}$> slip direction because the dislocations in the fcc mainly move in the direction of <11$\bar{2}$>. The generalized stacking fault energy calculation of fcc metals is mainly the calculation of generalized stacking fault energy curves in the direction of <11$\bar{2}$>. A shear deformation where a lattice plane glides over another can be produced by one or more dislocations. A particular shear deformation could be described by the definition of the glide plane and the direction of the deformation. Since GSFE contains the atomic position distribution characteristics of the slip surface, it is related to the crystal structure of the metal. The same slip system corresponds to different slip surfaces and slip paths, which would produce different GSFE curves.

For example, the <11$\bar{2}$> {111} shear system in a fcc crystal describes a relative displacement of two close-packed {111} planes along the <11$\bar{2}$> direction. It is known to us, for fcc crystals, <110> {111} shear deformation is the principal operation of the slip system. However, a dislocation with a Burger's vector $\vec{\mathrm{b}} = \frac{1}{2}[10\bar{1}]$ will dissociate into two partial

Shockley dislocations. The one is a leading partial with a Burgers vector $\vec{b_1} = \frac{1}{6}[11\bar{2}]$, the other is a trailing partial with a Burger's vector $\vec{b_2} = \frac{1}{6}[2\bar{1}\bar{1}]$, between which there will be an SF region with a lower mismatch energy. When the leading partial dislocations nucleate by overcoming the energy barrier γ_U, the trailing partials need to exceed this quantity. The dissociation process is described by the following reaction:

$$\frac{1}{2}[10\bar{1}] \rightarrow \frac{1}{6}[11\bar{2}] + \mathrm{SF} + \frac{1}{6}[2\bar{1}\bar{1}] \quad (1)$$

The dissociation can be understood from the GSFE surfaces for slip plane (1 1 1).

The GSFE plays an important role in the interpretation of the mechanical properties of metals. It effectively reflects the structural and process characteristics at the microscopic scale of metals in the form of energy. However, its sensitivity to small spatial scales makes determining GSFEs a major problem. As we all know, it is difficult to measure the GSFE curve through experiments except for a single point known as γ_I. Fortunately, we can turn to atomistic simulation, which has proved to be a powerful tool in many research fields. According to the different pseudopotentials, there are mainly two kinds of simulation methods to calculate the GSFE: one is the embedded atom method (EAM) with empirical potential [28–30], and the other is the first-principles method based on density functional theory (DFT). The emergence of empirical and first-principles atomic simulation methods has made the GSFE curve an important focus in the plastic deformation of bulk crystalline materials. However, due to the differences in the empirical potentials and the computational models, the GSFEs obtained by the EAM method are very different. The first-principles method does not depend on the empirical potential, and it is a relatively acceptable method for calculating the GSFE curve at present. There are three calculation models for the first-principles method that are used to calculate the GSFE: alias shear deformation [10], vacuum slab model [31,32] and anti-alias model [33].

As for the vacuum slab model, there is a strong interaction between the surface and the stacking fault (SF), which leads to some differences between the calculated results and the actual values. Furthermore, the extent of the calculation is greatly increased by the added vacuum layer. The alias shear deformation model has the advantages of simple modeling, and less calculation than the vacuum slab model. However, the condition of supercell symmetry must be relaxed, and the atoms cannot be relaxed during the process of first-principles calculations. It had been demonstrated in our previous article [34] that the factors atom position relaxation and surface interaction have a great influence on the ISFE calculations, and we developed a simple and effective model, including two periodic supercells with three typical generalized stacking fault structures, which would avoid these factors and obtain more accurate GSFEs than do the vacuum slab and alias shear methods.

The anti-alias method based on periodic supercells is a very effective method for calculating the GSFE of hcp crystals. However, when it is applied to an fcc crystal, two different GSFs will occur in the supercell during the sliding process (see Figure 1). Then, we can just obtain the superposition of the two GSFEs rather than the single GSFE. To separate the two GSFEs, the key is to extend the anti-alias model to the fcc crystal. The present work aims to extend the anti-alias model to compute the GSFE of fcc crystals in terms of the existing single analytic formula of GSFE via first-principles calculations. It will greatly decrease the amount of calculation and improve the calculation accuracy.

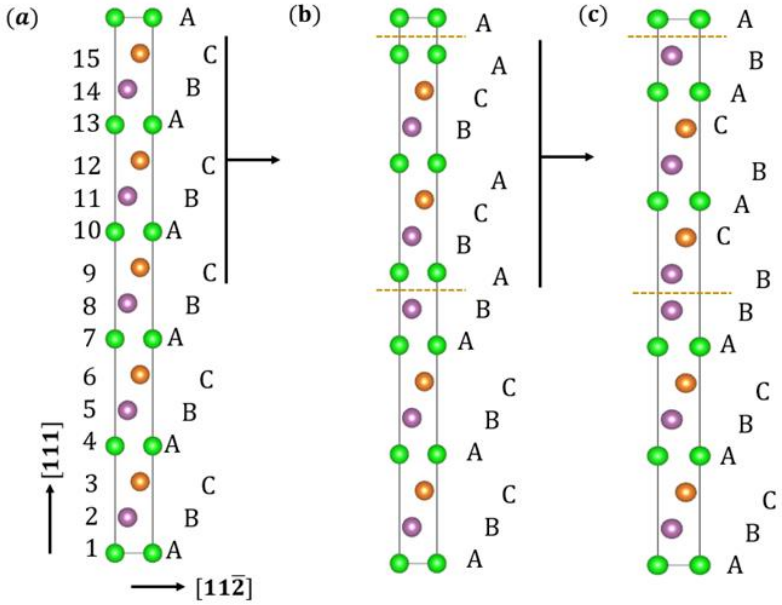


Figure 1. Selective schematic supercells to show the formation of two generalized stacking faults (i.e., the brown dash-dot lines) produced in the anti-alias of fcc crystal during the slip processes: (**a**) perfect structure; (**b**,**c**) stacking fault structure. The letters A, B and C represent the different layers of fcc crystals respectively, where green, purple and brown circles indicate atoms in layer A, B and C, respectively.

2. Computational Approach

The present calculations, based on density functional theory (DFT), were performed with the Vienna Ab initio Simulation Package (VASP) code [35]. The exchange-correlation functional was depicted by the generalized gradient approximation with the Perdew–Burke–Ernzerhof (PBE) [36]. In order to obtain accurate results, we performed accurate convergence tests on the K-point, plane wave energy cutoff energy and the size of the supercell. A Monkhorst–Pack grid of size of 23 × 23 × 2 was used to sample the surface of the Brillouin zone for the anti-alias model. A cutoff energy of 350 eV for the plane-wave basis ensures good accuracy. The Methfessel–Paxton scheme (ISMEAR = 1) is a good smearing approach for metal systems, and an entropy of less than 1 meV per atom is sufficient. After a careful convergence test, it was found that SIGMA = 0.2 was enough to support our calculations. The convergence criteria were reached by Hellmann–Feyman forces on all atomic sites smaller than 0.01 eV/Å, and the total energy of the convergent results was higher than 10^{-5} eV per supercell.

3. Results and Discussion

We take fcc Al as an example to discuss the separation process. First, we build up a 15-layer supercell, as shown in Figure 1a. Then, it is divided into the upper (9th~15th layer) and lower (1st~8th layer) parts along the (111) plane. Finally, make the two parts move relative to each other along (111) plane, and two different GSFs will occur in the supercell during the sliding process, as shown in Figure 1b,c. In the following sections, γ_1 and γ_2 are used to represent the upper and lower GSF, respectively. We take $\vec{u}$ as the sliding displacement vector, which represents the displacement of the upper half of the supercell relative to the lower half, $\vec{u} = 0$ represents sliding has not yet started; when sliding occurs, the sliding displacement vector $\vec{u} \neq 0$. The GSFE surface is the difference of the total energy before and after the relative slip of the supercell on the unit area [8], $\gamma\left(\vec{u}\right) = \left[E\left(\vec{u}\right) - E(0)\right]/A$, where E(0) and E($\vec{u}$) are the energies of the perfect lattice and the crystal with defect, respectively, and A is the sliding surface area.

According to the definition of GSFE, we can obtain the composite value of the two GSFEs ($\gamma_1 + \gamma_2$) of Al, Ni, Ag and Cu, and the result is shown in Figure 2. Actually, the analytic formula for the single GSFE (γ_1 or γ_2) is well known and has been widely used in the vacuum layer model [37,38]:

$$\begin{aligned}\gamma_{1,2}(u_x, u_y) = c_0 + c_1\left[\cos(2pu_x) + \cos\left(pu_x - qu_y\right) + \cos\left(pu_x + qu_y\right)\right] \\ + c_2\left[\cos\left(2pu_x - qu_y\right) + \cos\left(3pu_x - qu_y\right) + \cos\left(3pu_x + qu_y\right)\right] \\ + a_1\left[\sin(2pu_x) + \sin\left(qu_y - pu_x\right) - \sin\left(pu_x + qu_y\right)\right]\end{aligned} \quad (2)$$

where $p = 2\pi/(\sqrt{3}a_0)$, $q = 2\pi/a_0$, a_0 is the fcc lattice parameter, the coefficients c_0, c_1, c_2 and a_1 can be determined by fitting to the GSFE surface that can be obtained by our first-principles calculations. We observed that the superimposed GSFE curve is symmetric about the central position. Further observation of the atomic structure of the two GSFs, we also find that γ_1 and γ_2 equivalent to the two GSFs slip in opposite directions along <11$\bar{2}$>, i.e., $\gamma_1(u_x, u_y) = \gamma_2\left(\sqrt{3}a_0 - u_x, u_y\right)$. Based on the analytic formula of the single GSFE (i.e., Formula (2)) and the symmetry, we can derive the coefficient relation of γ_1 and γ_2 as follows:

$$c_0 = c_0',\ c_1 = c_1',\ c_2 = c_2',\ a_1 = -a_1' \quad (3)$$

where the letters with and without ' ' ' represent the coefficients of γ_1 and γ_2, respectively. According to Equations (2) and (3), we can obtain the expression of the composite GSFE in the anti-alias model:

$$\begin{aligned}\gamma(u_x, u_y) = \gamma_1(u_x, u_y) + \gamma_2(u_x, u_y) \\ = 2c_0 + 2c_1\left[\cos(2pu_x) + \cos\left(pu_x - qu_y\right) + \cos\left(pu_x + qu_y\right)\right] \\ + 2c_2\left[\cos\left(2pu_x - qu_y\right) + \cos\left(3pu_x - qu_y\right) + \cos\left(3pu_x + qu_y\right)\right]\end{aligned} \quad (4)$$

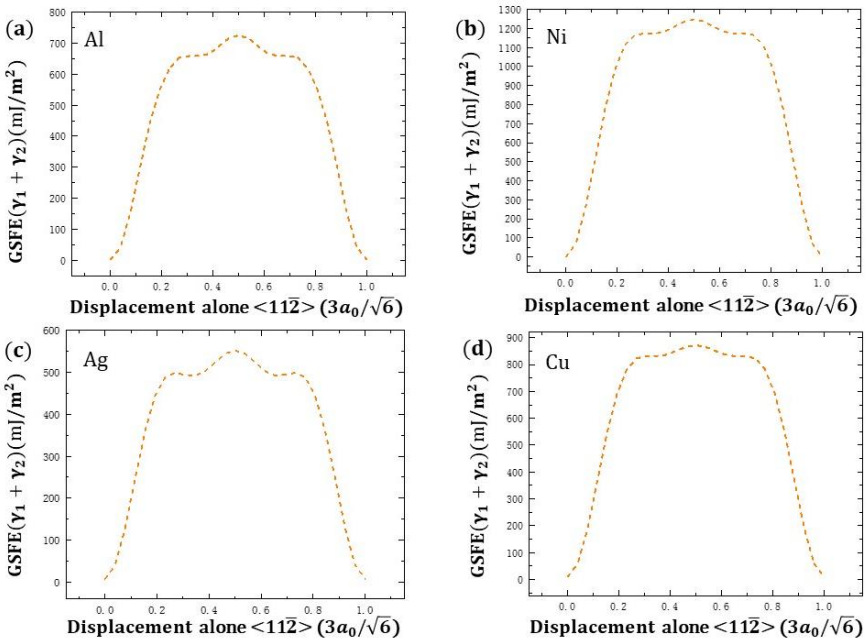


Figure 2. The composite generalized stacking fault energy ($\gamma_1 + \gamma_2$) of fcc Al, Ni, Ag and Cu obtained by using the anti-alias model as shown in (**a**), (**b**), (**c**) and (**d**), respectively, where γ_1 and γ_2 represent the values of the upper and lower generalized stacking fault energy. The sliding displacement ($3a_0/\sqrt{6}$) is set to 1.

In this section, the anti-alias method with a 15-layer (111) periodic supercell was applied to compute the generalized stacking fault energies of Al, Ag, Cu and Ni. We recorded the energy and the corresponding coordinate data when the upper and lower parts of the supercell slipped along the direction of <11$\bar{2}$> and <$\bar{1}$10>. Then, when the energy and coordinate data are substituted into Equation (4), we could obtain the three coefficients c_0, c_1 and c_2. In addition, we noticed that the point ($u_x = a_0/\sqrt{6}$,$u_y = 0$) on the curve γ_1 corresponding to the minimum energy, namely ISFE, and substitution of these data in the analytic formula for the single GSFE (i.e., Equation (2)) gives the value of the fourth coefficient a_1. So far, all the coefficients in the GSFE curve Equation (2) have been determined, and the results are illustrated in Table 1. In other words, two different GSFEs γ_1 and γ_2 in the fcc supercell model are completely separated.

Table 1. The fitted parameters c_0, c_1, c_2 and a_1 for the generalized stacking fault energy surface of fcc Al, Ni, Ag and Cu (mJ/m^2).

	c_0	c_1	c_2	a_1
Al	246.0	−63.0	−17.7	−60.6
Ni	479.8	−130.3	−26.1	177.0
Ag	208.7	−53.8	−14.5	85.1
Cu	329.2	−91.2	−16.8	144.5

By substituting the fitted parameters c_0, c_1, c_2 and a_1 into Equation (2) and taking the parameters' relation Equation (3) into account, the energy curves of γ_1 and γ_2 of the fcc metals Al, Ni, Ag and Cu are obtained, as shown in Figure 3. It is easily found that γ_1 and γ_2 are indeed two reverse slip SFs in < 11$\bar{2}$> direction, and curves γ_1 and γ_2 intersect at the point of 1.5 b_p, where b_p represents Burger's vector. It is interesting to note that the composite value of γ_1 and γ_2 at intersection point 1.5 b_p corresponds to the maximum value point in Figure 2 (i.e., $(\gamma_1+\gamma_2)_{max}$ = 726 mJ/m^2). At the same time, the curves γ_1 and γ_2 are symmetrical about point 1.5b_p. The symmetry alone in the <11$\bar{2}$> {111} direction of the two stacking faults in our anti-alias method is well demonstrated.

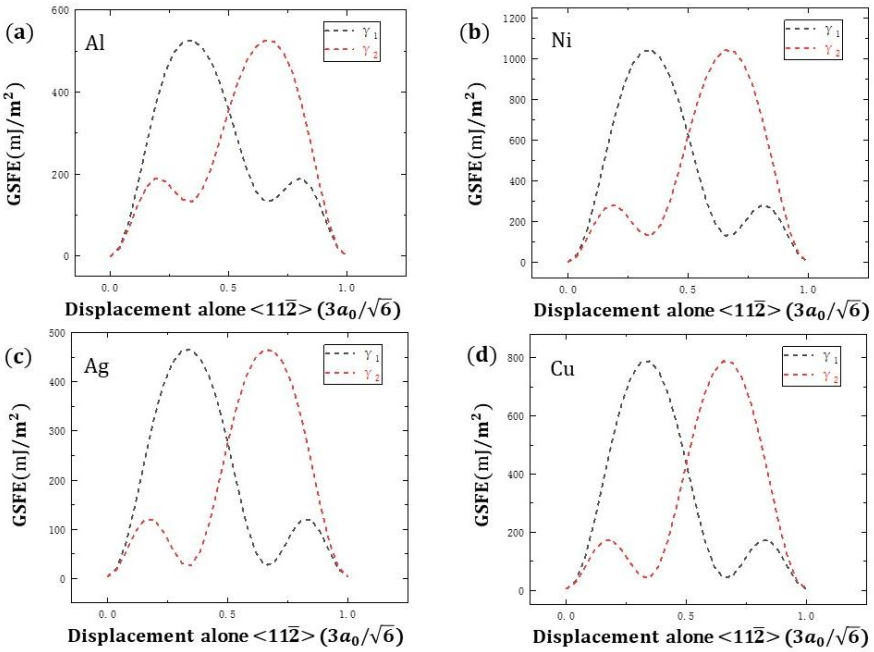


Figure 3. The separated upper and lower generalized stacking fault energy curves of fcc metals (γ_1 and γ_2) obtained by using the anti-alias model: (**a**–**d**) represent the metals Al, Ni, Ag and Cu, respectively, where a_0 is the lattice constant, and the sliding displacement ($3a_0/\sqrt{6}$) is set to 1.

In order to verify the separation results, we further compare the data in Figures 2 and 3 in detail. As shown in Table 2, we list some of the composite values of the two generalized stacking fault energies $(\gamma_1 + \gamma_2)$ in Figure 2 and the single generalized stacking fault energy γ_1, γ_2 in Figure 3 of Al (as a specific example), where the sliding displacement $(3a_0/\sqrt{6})$ is set to 1. It is clearly shown that γ_1 and γ_2 are two reverse-slip stacking faults. For instance, the ISFE γ_I (133 mJ/m^2) along <11$\bar{2}$> direction of curve γ_1 and γ_2 is reflected at a sliding displacement of 9/26 and 17/26 (i.e., the sliding displacement is about $1b_p$), respectively. It also can be seen from Table 2 that the value of USFE is 189 mJ/m^2, which corresponds to the sliding displacement 5/26 (a little more than one-half of the partial Burger's vectors). The calculated result shows that the offset of the actual displacements from the one-half of the partial Burger's vector is different, but the offset is relatively small, so it will not affect the calculation result too much. Furthermore, the summation value γ_3 is basically equal to the composite value of $(\gamma_1 + \gamma_2)$. It demonstrates the reliability of our methods.

Table 2. The composite value of the two generalized stacking fault energies $(\gamma_1 + \gamma_2)$ in Figure 2 and γ_1, γ_2 in Figure 3 of fcc Al. γ_3 is the sum of γ_1 and γ_2 (i.e., $\gamma_3 = \gamma_1 + \gamma_2$). The sliding displacement $(3a_0/\sqrt{6})$ is set to 1, where a_0 is the lattice constant, and the unit is Å.

Sliding Displacement	γ_1 (mJ/m^2)	γ_2 (mJ/m^2)	γ_3 (mJ/m^2)	$(\gamma_1+\gamma_2)$ (mJ/m^2)
1/26	20	19	39	41
2/26	82	67	149	151
3/26	174	125	299	300
4/26	277	170	447	444
5/26	372	189	561	550
6/26	448	183	630	620
7/26	498	159	657	654
8/26	523	137	660	659
9/26	526	133	659	659
10/26	511	158	669	667
11/26	477	210	687	690
12/26	425	281	705	716
13/26	357	357	713	726
14/26	281	425	705	716
15/26	210	477	687	690
16/26	158	511	669	667
17/26	133	526	659	659
18/26	137	523	660	659
19/26	159	498	657	654
20/26	183	448	630	620
21/26	189	372	561	550
22/26	170	277	447	444
23/26	125	174	299	300
24/26	67	82	149	151
25/26	19	20	39	41
1	0	0	0	0

In order to test the correctness of our methods, we listed two important characteristic energies γ_I and γ_U obtained by our anti-alias model in Table 3 and compared them with the reported results. It was found that the results we obtained are in good agreement with those in other studies. The value of ISFE follows the order: γ(Ag) > γ(Ni) > γ(Cu) > γ(Ag), where the ISFE of Al and Ni is similar (about 130 mJ/m^2). However, the USFE of Ni is 280 mJ/m^2, which is much higher than that of Al (189 mJ/m^2). There are some differences between our calculated results and the existing literature results, which could be caused by the differences in the calculated model, the size of the supercell, the different parameter settings, etc., and it can be considered that our results are in a reasonable range.

It is known to us that the deformation mechanism in a simulation cannot be explained by the absolute value of γ_I alone in the <11$\bar{2}$> {111} direction. The dislocation activity in

a simulation is dominated by extended partials or full dislocations traveling through the grains in the simulated time span, which must be understood in terms of γ_I/γ_U. Rice et al. [39] showed that the critical stress for nucleation of the trailing partial will be a function of $\gamma_U - \gamma_I$. Then, a large difference between γ_I and γ_U promotes splitting of full dislocations into partials and makes it easier to generate stacking faults. So, we also list the ratios of γ_I/γ_U in Table 3. If, for a metal with a low value of γ_I/γ_U, the energy increase necessary for nucleating the trailing partial is substantial, it indicates a greater tendency to full dislocation dissociation into partials, then the extended partial dislocations will be observed more easily. If a metal has a high value of γ_I/γ_U, although the stacking-fault energy is higher, full dislocation will be easier to observe. The ratios of γ_I/γ_U for four metals Al, Ni, Ag and Cu are 0.7, 0.46, 0.21 and 0.24, respectively. The order of γ_I/γ_U from low to high is as follows: Ag (0.21) < Cu (0.26) < Ni (0.46) < Al (0.7). As for Al, it may be the most impossible one to create partial dislocation, but it is the easiest one to create full dislocation because it has the highest γ_I/γ_U value of the four metals. It has been verified in simulations that extended partial dislocations in Cu are the predominant deformation mechanism at nanocrystalline grains [40]. Similarly, the γ_I/γ_U value of Cu obtained by the anti-alias model is only 0.24.

Table 3. The calculated γ_I, γ_U and the ratios of γ_I /γ_U of fcc Al, Ni, Ag and Cu. All values are in units of (mJ/m^2).

Model	γ_I	γ_U	γ_I/γ_U
Al	133	189	0.7
	130 [41], 146 [42], 158 [43]	162 [41], 178 [42], 175 [43]	
Ni	129	280	0.46
	110 [44], 120–130 [45], 132 [33]	305 [33], 278 [42], 273 [41]	
Ag	26	119	0.21
	17 [37], 25.9 [4], 18 [41]	93 [24], 111 [37], 190 [46]	
Cu	42	171	0.24
	43 [37], 51 [47], 40.5 [9]	158 [31], 161 [9], 175 [37]	

4. Conclusions

In summary, the GSFE curve and the associated characteristic energies can be used to model a vast number of phenomena linked to dislocation slipping, plastic deformation, crystal growth, phase transition and so on. The vacuum slab model and the alias shear deformation model are widely used to calculate the GSFE of fcc crystals. However, the extent of the calculation is greatly increased by the added vacuum layer. More importantly, there is a strong interaction between the surface and the stacking fault (SF), which leads to some differences between the calculated results and the actual value. As for the alias shear deformation model, the condition of supercell symmetry must be relaxed, and the atoms cannot be relaxed during the process of first-principles calculations, which has a certain influence on the calculation accuracy. In this study, we fully considered the accuracy of results and the computational complexity and aimed to develop an efficient computational method to calculate the GSFE of fcc crystals. We present ab initio calculations on the generalized stacking fault energy surfaces for the closed-packed (1 1 1) plane in fcc metals Al, Ni, Ag and Cu. The density functional theory (DFT) with the Perdew–Burke–Ernzerhof (PBE) was used. Based on the symmetry of those two GSFs and the existing single analytic formula of GSFE, two GSFEs γ_1 and γ_2 are completely separated, and the anti-alias model is successfully extended to fcc crystals. Finally, the new model is verified by being used to calculate the GSFE of fcc Al, Ni, Ag and Cu.

Author Contributions: Conceptualization, L.L.; Formal analysis, D.F. and Q.Z.; Investigation, T.F. and M.H.; Methodology, T.F. and M.H.; Software, Q.Z.; Supervision, L.L.; Visualization, D.F.; Writing—original draft, D.F.; Writing—review and editing, L.L. All authors have read and agreed to the published version of the manuscript.

Funding: This work was supported by the National Natural Science Foundation of China (Nos. 51701243), the Hunan Provincial Natural Science Foundation of China (No. 2019JJ40544), the Excellent Youth Foundation of the Educational Committee of Hunan Provincial (No. 19B587), and the PhD Research Startup Foundation of the Central South University of Forestry and Technology (No. 2017YJ020). The numerical results in this paper have been computed on the supercomputing system of the National Supercomputing Center in Changsha.

Data Availability Statement: The data presented in this study are available on request from the corresponding author. The data are not publicly available due to privacy or ethical restrictions.

Conflicts of Interest: The authors declare no conflict of interest.

References

1. Cheng, Z.; Zhou, H.F.; Lu, Q.H.; Gao, H.J.; Lu, L. Extra strengthening and work hardening in gradient nanotwinned metals. *Science* **2018**, *362*, 559. [CrossRef]
2. Zhao, F.; Wang, L.; Fan, D.; Bie, B.X.; Zhou, X.M.; Suo, T.; Li, Y.L.; Chen, M.W.; Liu, C.L.; Qi, M.L.; et al. Macrode formation Twins in Single-Crystal Aluminum. *Phys. Rev. Lett.* **2016**, *116*, 075501. [CrossRef]
3. Edalati, K.; Akama, D.; Nishio, A.; Lee, S.; Yonenaga, Y.; Cubero-Sesin, J.M.; Horita, Z.J. Influence of dislocation–solute atom interactions and stacking fault energy on grain size of single-phase alloys after severe plastic deformation using high-pressure torsio. *Acta Mater.* **2014**, *69*, 68–77. [CrossRef]
4. Cai, T.; Zhang, Z.J.; Zhang, P.; Yang, J.B.; Zhang, Z.F. Competition between slip and twinning in face-centered cubic metals. *J. Appl. Phys.* **2014**, *116*, 163512. [CrossRef]
5. Chowdhury, P.B.; Sehitoglu, H.; Rateick, R.G. Predicting fatigue resistance of nano-twinned materials: Part I—Role of cyclic slip irreversibility and Peierls stress. *Int. J. Fatigue* **2014**, *68*, 277–291. [CrossRef]
6. Meyers, M.A.; Benson, D.J.; Vöhringer, O.; Kad, B.K.; Xue, Q.; Fu, H.H. Constitutive description of dynamic deformation: Physically-based mechanisms. *Mater. Sci. Eng. A* **2002**, *322*, 194–216. [CrossRef]
7. Nishikawa, O.; Walko, R.J. Field ion microscopical observation of twinning in iridium induced by a mechanical contact. *Acta Metall.* **1971**, *19*, 1163–1168. [CrossRef]
8. Vítek, V. Intrinsic stacking faults in body-centred cubic crystals. *Philos. Mag.* **1968**, *18*, 773–786. [CrossRef]
9. Zhao, D.D.; Løvvik, O.M.; Marthinsen, K.; Li, Y.J. Impurity effect of Mg on the generalized planar fault energy of Al. *J. Mater. Sci.* **2016**, *51*, 6552–6568. [CrossRef]
10. Wang, Z.P.; Xiao, H.; Ma, L.; Fan, T.W.; Tang, P.Y. Effects of rare-earth elements on twinning deformation of Al alloys from first-principles calculations. *Solid State Commun.* **2022**, *356*, 114946. [CrossRef]
11. Liu, L.H.; Chen, J.H.; Fan, T.W.; Shang, S.L.; Shao, Q.Q.; Yuan, D.W.; Dai, Y. The stability of deformation twins in aluminum enhanced by alloying elements. *J. Mater. Sci. Technol.* **2019**, *35*, 2625–2629. [CrossRef]
12. Schönecker, S.; Li, W.; Vitos, L.; Li, X.Q. Effect of strain on generalized stacking fault energies and plastic deformation modes in fcc-hcp polymorphic high-entropy alloys: A first-principles investigation. *Phys. Rev. Mater.* **2021**, *5*, 075004. [CrossRef]
13. Janković, B.; Joksimović, T.; Stare, J.; Losev, E.; Zemtsova, V.; Srčič, S.; Boldyrev, E. Quantification and modeling of nanomechanical properties of chlorpropamide α, β, and γ conformational polymorphs. *Eur. J. Pharm. Sci.* **2017**, *110*, 109–116. [CrossRef] [PubMed]
14. Arkhipov, S.G.; Sherin, P.S.; Kiryutin, A.S.; Lazarenko, V.A.; Tantardini, C. The Role of S-bond in Tenoxicam Keto-Enolic Tautomerization. *CrystEngComm* **2019**, *36*, 5392–5401. [CrossRef]
15. Arkhipov, S.G.; Rychkov, D.A.; Pugachevc, A.M.; Boldyrevaa, E.V. New hydrophobic L-amino acid salts: Maleates of L-leucine, L-isoleucine and L-norvaline. *Acta Crystallogr. C Struct. Chem.* **2015**, *71*, 584–592. [CrossRef]
16. Asanbaeva, N.B.; Rychkov, D.A.; Tyapkin, P.Y.; Arkhipov, S.G.; Uvarov, N.F. The unique structure of $[(C_4H_9)_4N]_3[Pb(NO_3)_5]$—One step forward in understanding transport properties in tetra-n-butylammonium-based solid electrolytes. *Struct. Chem.* **2021**, *32*, 1261–1267. [CrossRef]
17. Desta, I.T.; Chizhik, S.A.; Sidelnikov, A.A.; Karothu, D.P.; Boldyreva, E.V.; Naumov, P. Mechanically Responsive Crystals: Analysis of Macroscopic Strain Reveals "Hidden" Processes. *J. Phys. Chem. A* **2020**, *124*, 300–310. [CrossRef]
18. Tantardini, C.; Arkhipov, S.G.; Cherkashina, K.A.; Kil'met'eva, A.S.; Boldyreva, E.A. Crystal structure of a 2:1 co-crystal of meloxicam with acetylendicarboxylic acid. *Acta Crystallogr.* **2016**, *72*, 1856–1859. [CrossRef]
19. Tantardini, C.; Arkipov, S.G.; Cherkashina, K.A.; Kil'met'ev, A.S.; Boldyreva, E.V. Synthesis and crystal structure of a meloxicam co-crystal with benzoic acid. *Struct. Chem.* **2018**, *29*, 1867–1874. [CrossRef]
20. Vaid, A.; Wei, D.; Bitzek, E.; Nasiri, S.; Zaiser, M. Pinning of extended dislocations in atomically disordered crystals. *Acta Mater.* **2022**, *236*, 118095. [CrossRef]
21. Shih, M.; Miao, J.S.; Mills, M.; Ghazisaeidi, M. Stacking fault energy in concentrated alloys. *Nat. Commun.* **2021**, *12*, 3590. [CrossRef] [PubMed]
22. Qiu, S.; Zheng, G.P.; Jiao, Z.B. Alloying effects on phase stability, mechanical properties, and deformation behavior of CoCrNi-based medium-entropy alloys at low temperatures. *Intermetallics* **2022**, *140*, 107399. [CrossRef]
23. Van Swygenhoven, H.; Derlet, P.M.; Froseth, A.G. Stacking fault energies and slip in nanocrystalline metals. *Nat. Mater.* **2004**, *3*, 399–403. [CrossRef] [PubMed]

24. Tadmor, E.B.; Bernstein, N. A First-Principles Measure for the Twinnability of FCC Metals. *J. Mech. Phys. Solids* **2004**, *52*, 2507–2519. [CrossRef]
25. Achmad, T.L.; Fu, W.X.; Chen, H.; Zhang, C.; Yang, Z.G. First-principles calculations of generalized-stacking-fault-energy of Co-based alloys. *Comput. Mater. Sci.* **2016**, *121*, 86–96. [CrossRef]
26. Liu, L.L.; Wang, R.; Wu, X.Z.; Gan, L.Y.; Wei, Q.Y. Temperature effects on the generalized planar fault energies and twinnabilities of Al, Ni and Cu: First principles calculations. *Comput. Mater. Sci.* **2014**, *88*, 124–130. [CrossRef]
27. Asaro, R.J.; Suresh, S. Mechanistic models for the activation volume and rate sensitivity in metals with nanocrystalline grains and nano-scale twins. *Acta Mater.* **2005**, *53*, 3369–3382. [CrossRef]
28. Aitken, Z.H.; Sorkin, V.; Yu, Z.G.; Chen, S.; Wu, Z.X.; Zhang, Y.W. Modified embedded-atom method potentials for the plasticity and fracture behaviors of unary fcc metals. *Phys. Rev. B* **2021**, *103*, 094116. [CrossRef]
29. Xu, L.B.; Casillas-Trujillo, L.; Gao, Y.F.; Xu, H.X. Compositional effects on stacking fault energies in Ni-based alloys using first-principles and atomistic simulations. *Comput. Mater. Sci.* **2021**, *197*, 110618. [CrossRef]
30. Chang, L.; Liu, X.R.; Zhao, J.L.; Zhou, C.Y. Effect of interatomic potential on modelling fracture behavior in hcp titanium: A molecular dynamics study. *J. Mater. Res. Technol.* **2022**, *17*, 2118–2133. [CrossRef]
31. Qing, D.; Luo, Z.; Zhu, H.; Wang, L.Y.; Ying, T.; Jin, Z.H.; Li, D.J.; Ding, W.J.; Zeng, X.Q. Basal-plane stacking-fault energies of Mg alloys: A first-principles study of metallic alloying effects. *J. Mater. Sci. Technol.* **2018**, *34*, 1773–1780.
32. Zhao, S.J.; Malcolm Stocks, G.; Zhang, Y.W. Stacking fault energies of face-centered cubic concentrated solid solution alloys. *Acta Mater.* **2017**, *134*, 334–345. [CrossRef]
33. Shang, S.L.; Wang, W.Y.; Zhou, B.C.; Wang, Y.; Darling, K.A.; Kecskes, L.J.; Mathaudhu, S.N.; Liu, Z.K. Generalized stacking fault energy, ideal strength and twinnability of dilute Mg-based alloys: A first-principles study of shear deformation. *Acta Mater.* **2014**, *67*, 168–180. [CrossRef]
34. Liu, L.H.; He, M.D.; Li, J.B.; Peng, X.F.; Chen, H.; Wang, Z.P.; Fan, T.W. A novel simplified model for measuring the twinnability of face-centred-cubic metals. *Philos. Mag. Lett.* **2020**, *100*, 63–73. [CrossRef]
35. Kresse, G.; Furthmüller, J. Efficient iterative schemes for ab initio total-energy calculations using a plane-wave basis set. *Phys. Rev. B* **1996**, *54*, 11169–11186. [CrossRef]
36. Arshad Javid, M.; Khan, Z.U.; Mehmood, Z.; Nabi, A.; Hussain, F.; Imran, M.; Nadeem, N.; Anjum, N. Structural, electronic and optical properties of $LiNbO_3$ using GGA-PBE and TB-mBJ functionals: A DFT study. *Int. J. Mod. Phys. B* **2018**, *32*, 1850168. [CrossRef]
37. Wu, X.Z.; Wang, R.; Wang, S.F.; Wei, Q.Y. Ab initio calculations of generalized-stacking-fault energy surfaces and surface energies for FCC metals. *Appl. Surf. Sci.* **2010**, *256*, 6345–6349. [CrossRef]
38. Kibey, S.; Liu, J.B.; Curtis, M.J.; Johnson, D.D.; Sehitoglu, H. Effect of nitrogen on generalized stacking fault energy and stacking fault widths in high nitrogen steels. *Acta Mater.* **2006**, *54*, 2991–3001. [CrossRef]
39. Rice, J.R. Dislocation Nucleation from a Crack Tip: An Analysis Based on the Peierls Concept. *J. Mech. Phys. Solids* **1992**, *40*, 239–271. [CrossRef]
40. Schiøtz, J.; Jacobsen, K.W. A Maximum in the Strength of Nanocrystalline Copper. *Science* **2003**, *301*, 1357. [CrossRef]
41. Kibey, S.; Liu, J.B.; Johnson, D.D.; Sehitoglu, H. Predicting twinning stress in fcc metals: Linking twin-energy pathways to twin nucleation. *Acta Mater.* **2007**, *55*, 6843–6851. [CrossRef]
42. Brandl, C.; Derlet, P.M.; Van Swygenhoven, H. General-stacking-fault energies in highly strained metallic environments: Ab initio calculations. *Phys. Rev. B* **2007**, *76*, 054124. [CrossRef]
43. Ogata, s.; Li, j.; Yip, S. Ideal pure shear strength of aluminum and copper. *Science* **2002**, *298*, 807–811. [CrossRef]
44. Donald, J. Siegel. Generalized stacking fault energies, ductilities, and twinnabilities of Ni and selected Ni alloys. *Appl. Phys. Lett.* **2005**, *87*, 121901.
45. Carter, C.B.; Holmes, S. The stacking-fault energy of nickel. *Philos. Mag.* **1977**, *35*, 1161. [CrossRef]
46. Kioussis, N.; Herbranson, M.; Collins, E.; Eberhart, M.E. Topology of Electronic Charge Density and Energetics of Planar Faults in fcc Metals. *Phys. Rev. Lett.* **2002**, *88*, 125501. [CrossRef]
47. Hartford, J.; von Sydow, B.; Wahnström, G.; Lundqvist, B.I. Peierls barriers and stresses for edge dislocations in Pd and Al calculated from first principles. *Phys. Rev. B* **1998**, *58*, 2487. [CrossRef]

Disclaimer/Publisher's Note: The statements, opinions and data contained in all publications are solely those of the individual author(s) and contributor(s) and not of MDPI and/or the editor(s). MDPI and/or the editor(s) disclaim responsibility for any injury to people or property resulting from any ideas, methods, instructions or products referred to in the content.